Letter

Depressurization-induced drop breakup through bubble growth

Christophe Pirat,[1,*] Cécile Cottin-Bizonne,[1] Choongyeop Lee,[2]
Stella M. M. Ramos,[1] and Olivier Pierre-Louis[1]
[1]Institut Lumière Matière, Université de Lyon, Université Claude Bernard Lyon 1, CNRS UMR5306, Campus de la Doua, F-69622 Villeurbanne, France
[2]Department of Mechanical Engineering (Integrated Engineering Program), Kyung Hee University, Yongin 17104, Republic of Korea

(Received 28 September 2022; revised 20 January 2023; accepted 3 August 2023; published 19 September 2023)

Drop breakup is often associated with violent impacts onto targets or fast inner bubble growth consecutive to phase change. We report on a well-controlled drop breakup experiment where bubble growth is triggered by the decrease of the ambient pressure. The drop initially sits on a textured hydrophobic surface at controlled temperature, and a bubble grows from the center of the liquid-solid interface. We find a transition from top-breakup to triple-line breakup depending on the initial contact angle of the drop. A minimal model based on inertial dynamics and constant bubble pressure is proposed. It quantitatively captures the growth of the bubble and the distinction between top or triple-line breakup. However, the model only provides an upper bound for the breakup time.

DOI: 10.1103/PhysRevFluids.8.L091601

Drop dynamics is central in many wetting processes, for instance in the fields of chemical deposition, surface cleaning, and heat transfer optimization, although most of the time controlling and manipulating the drops is challenging. In this context, numerous works have been devoted to drop jump from solid surfaces. Selected examples are the takeoff of small evaporating leidenfrost droplets [1], coalescence-induced jump [2–4], and catapult-like ejection [5,6]. Also Ref. [7] reports on spontaneous trampoline-like bouncing and icing on superhydrophobic surfaces at low surrounding pressure. Another possible fast event at solid surfaces is bubble formation. Bubble nucleation in a liquid can occur if suitable thermodynamic conditions are met [8–10]. At solid surfaces the local wetting conditions are known to play a role [11,12]. Drop impacts and jumps can also involve bubble formation. Indeed, it has been reported that a bubble can be trapped beneath an impacting drop on a solid surface [13]. Recently, several works have been devoted to the jump and the bouncing of drops associated with vapor bubble formation at high surface temperature (hydrogel drops on smooth surface [14] or water drop on superhydrophilic material [15]), or in a low-pressure environment: strong bouncing on a smooth hydrophilic surface [16] and so-called magic carpet break-up at low impact velocity [17].

In the present Letter, we study the dynamics of sessile water drops on hydrophobic surfaces in a transparent glass chamber under variable substrate temperature and surrounding low-air-pressure conditions (Fig. 1). We focus on experiments with water drops sitting on surfaces decorated with a micron-sized regular pattern, i.e., a hydrophobic configuration with air trapped beneath the drops. This configuration allows us to achieve fast bubble growth in moderate pressure and temperature ranges, i.e., in conditions that are easily achievable. Bubble growth is experimentally driven by the

*christophe.pirat@univ-lyon1.fr

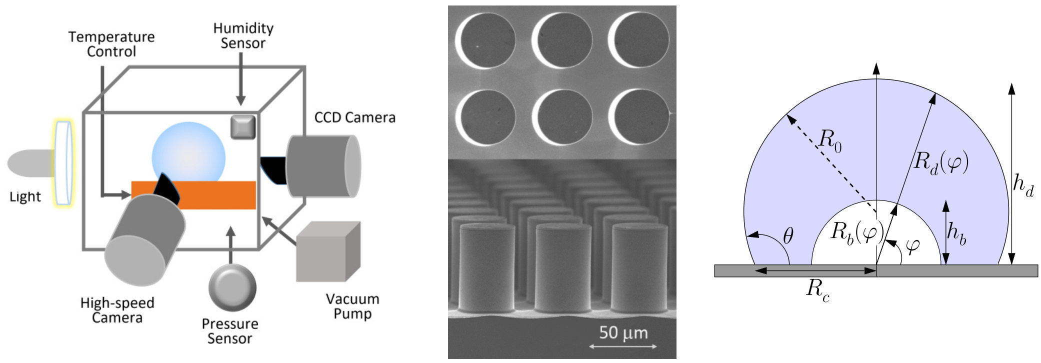

FIG. 1. Sketch of the experimental setup, SEM (top and side) views of a patterned surface used for the experiment, and schematic of the drop and the bubble on a heated micro-patterned surface, with notations as used throughout this Letter.

decrease of ambient pressure, while the temperature is fixed. This method is to be compared with the indirect decrease of pressure induced by evaporation used in Ref. [12]. In our experimental setup the temperature is adjusted through a heating element underneath the substrate and controlled with a Proportional-integral-derivative controller. Moreover, pressure control is achieved using a vacuum pump in combination with a pressure sensor with 0.05% accuracy.

The micro-patterned surface consists of a square array of cylindrical microposts 36 µm in diameter with a center-to-center distance of 50 µm, which leads to a solid-liquid contact fraction of 0.4 (see Fig. 1). The surface is treated with a silane-based hydrophobic coating. Details on the surface fabrication are given in the Supplemental Material [18]. The initial static contact angle (CA) obtained from pictures taken with a side view Charge-coupled device camera is $\theta = (132 \pm 3)^\circ$ at 50 °C under atmospheric pressure. It decreases slightly by 1° or 2° on substrates heated at 80 °C, consistently with the small variation of the adhesion energy in this temperature range Ref. [19].

Prior to each experiment the substrate temperature is fixed in the range 30–80 °C. An ultrapure water drop of fixed radius $R_0 \approx 1.25$ mm, initially at room temperature, is deposited on the substrate enclosed in the glass chamber at atmospheric pressure. Then the pressure inside the chamber is reduced in a few seconds down to 2 kPa while the drop dynamics is captured from the side with a high-speed camera (Photron SA4) operating in the range 1–30 kfps. The temporal evolution of the pressure inside the chamber is recorded and later synchronized with the camera time (see details in the Supplemental Material [18]). In such conditions, the substrate temperature appears as a static control parameter in our experiments.

As the drop is gently deposited on the surface, it remains mostly in the so-called fakir state, i.e., it is only in contact with the top of the pillars [20]. In all the experiments, we apply a decrease of the background pressure reaching vanishing pressures in a few seconds. This accelerates the evaporation rate significantly. Several scenarios are observed depending on the substrate temperature. (i) At low surface heating (below 50 °C), the pressure decrease can induce the freezing of the drop (see Fig. 2 (left) and [7,21]). (ii) For a higher surface temperature, the drop may experience a spontaneous vertical oscillation with the bottom partially pinned at the surface and an oscillation period of 20–30 ms. The anchoring of the drop at the surface is interpreted as a consequence of a localized fakir-to-Wenzel transition, i.e., a partial collapse of the Cassie-Baxter state has occurred [see Fig. 2 (center)]. It is assumed that the vapor flow under the drop amplifies the fundamental mode of period $\sim(\rho_L R_0^3/\gamma)^{1/2} = 30$ ms of the order of those measured in the experiments. This is similar to what is observed for trampolining drops in Ref. [7] which reports on spontaneous trampoline-like bouncing behavior, and icing, on superhydrophobic surfaces at low pressure but room temperature. Interestingly, bubble growth is not observed in Ref. [7] (superhydrophobic surface), while it is observed on textured superhydrophilic [15], smooth [16], and hydrophobic (the present study)

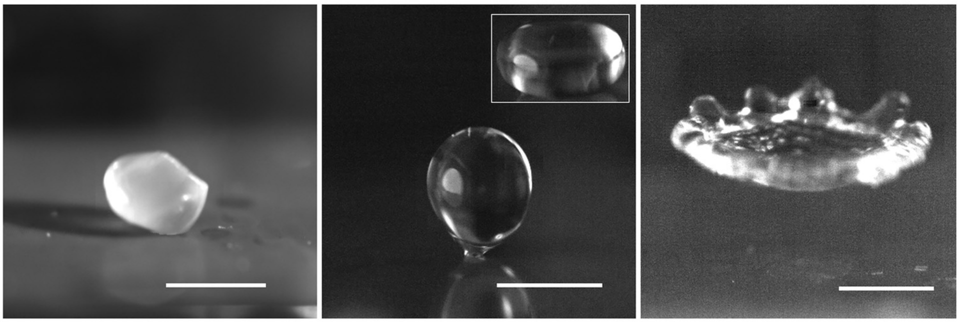

FIG. 2. From left to right at increasing surface temperature: Drop freezing, here at 30 °C; drop vertical oscillation at its maximal elongation (note the flattened shape of the drop in the inset, as it appears 15 ms later), here at 50 °C; and drop takeoff after a fast growing bubble has formed, here at 65 °C. The bars indicate 3 mm.

configurations. This indicates that a minimum adhesion might be required for a bubble to grow, as it prevents a vapor cushion from detaching the drop from the solid at an early stage. In this Letter, we focus on the fast growing bubble dynamics. (iii) For temperatures above 50 °C, and when the falling surrounding pressure in the chamber P reaches some threshold value P_{th}, a bubble starts to expand at the liquid-solid interface in the middle of the drop base, where the pressure is maximum by symmetry. Please note that a minimal adhesion is required for the system to sustain bubble growth instead of vapor cushion formation under the drop Fig. 2 (right). In this Letter, based on our optical observations, we focus on bubble growth rather than on the initial mechanism at the origin of the bubble formation.

In this latter regime, the pressure inside the chamber is constant at P_{th} during the whole bubble growth [18]. The typical bubble front velocity is about 1 m/s and the drop break up takes around 1 ms (see Fig. 3). As a consequence, the drop inflates and the contact line is moved outward. Then, as the bubble reaches the contact line, the drop leaves the solid surface in an upward motion [see in the Supplemental Material [18]; Fig 3 (right)], referred to as *takeoff* hereafter. Typically, in our experiments the detachment happens half a millisecond after the bubble expansion has started while the complete evaporation time of a drop would be larger than a second. The side view snapshot in Fig. 3 shows the bubble growth, the drop takeoff, and later a transitorily flattened shape during the ascending motion. Note that the clearly visible capillary waves could be coupled to the detachment and takeoff dynamics [22].

Because of the optical refraction at the curved drop surface, the bubble looks flattened and becomes visible only after a delay. Taking into account the refraction, the actual bubble height together with the time at which it starts expanding (chosen as the initial time $t = 0$) are inferred (see Supplemental Material [18]). Further, we measure the evolution of the bubble height h_b, the drop height h_d, and the radius of the drop base R_c, as a function of time for several substrate temperatures.

To discuss the last scenario presented above (bubble growth followed by the takeoff of the drop), we design a minimal model. Considering that the velocity of the radial expansion of the bubble is about 1 m/s, we assume that the motion of the liquid is dominated by inertial effects, neglecting viscous dissipation and surface tension. Indeed, for a drop radius of 1 mm, the Weber number We, which compares the kinetic energy to surface tension effects is We $\approx$50, and the Reynolds number Re which compares inertial and viscous forces is Re $\approx 10^3$. When considering small bubble radii, the Weber number decreases up to We $\approx$ 1 for radii around 20 μm, i.e., similarly to the gap between micropillars. As mentioned above, we focus on bubble growth after the formation of the bubble when its size is much larger than the size of the microstructure, and we can therefore safely neglect the effect of surface tension. We also neglect friction between the liquid and the substrate, as expected in the limit of a fakir state with a very small contact fraction. We then proceed with further simplifications, assuming that the hydrodynamic flow is purely radial from the initial point

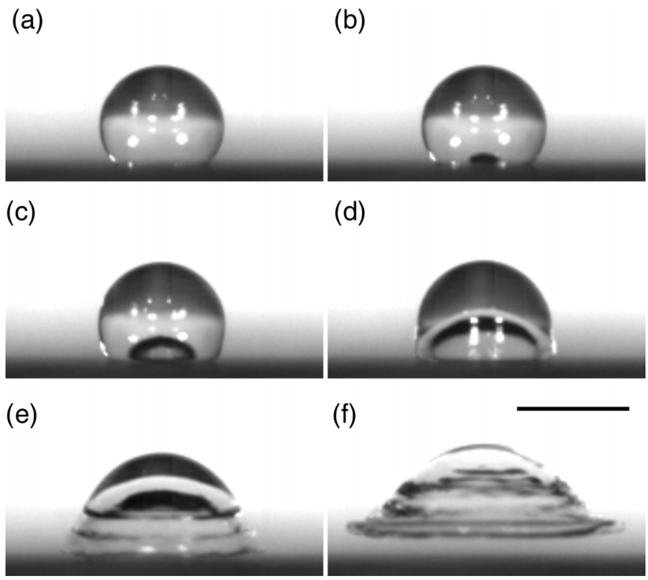

FIG. 3. Side view snapshots from a representative experiment. The vapor bubble, visible at the base of the drop, grows until the drop leaves the surface in an ascending motion. Surface temperature 65 °C and ambient pressure 15 kPa. [(a)–(f)] $t = 0$, 0.07, 0.2, 0.4, 0.67, and 1.00 ms. Takeoff happens between (d) and (e). Scale bar: 2 mm.

of formation of the bubble in the center of the liquid-substrate interface and that the difference of pressure ΔP between the interior of the bubble and the chamber is a constant denoted $\Delta P_{\rm gr}$. An evolution law for the bubble and drop shapes is obtained from the balance between variation of the kinetic energy and the work exerted by excess pressure at the surface of the bubble. Details are reported in the Supplemental Material [18]. The drop and bubble shapes are assumed to be axisymmetric around the vertical axis passing through the center of the drop-substrate contact zone.

The model provides a prediction for the bubble interface position $R_b(\varphi, t)$ and the drop surface position $R_d(\varphi, t)$ measured from the center of the contact zone at the surface of the substrate. The distance $R_b(\varphi, t)$ depends on time and on the angle $0 \leqslant \varphi \leqslant \pi/2$ from the horizontal substrate plane. As expected, and previously derived in the Rayleigh-Plesset model [9,23], our model predicts that the bubble is a spherical cap in the early stage of its growth, with a radius that is independent of φ,

$$R_b(\varphi, t) \approx \left(\frac{2\Delta P_{\rm gr}}{3\rho_L}\right)^{1/2} t, \tag{1}$$

where ρ_L is the mass density of the liquid.

At later times, the growth of the bubble accelerates due to the finite size of the drop. This acceleration is larger in the directions where the thickness of the liquid is smaller. The model actually predicts that the acceleration leads to a divergence in finite time at $t = t_0(\varphi)$ for a given angle φ. At the divergence, the bubble and drop radii diverge [i.e., $R_b(\phi, t_0(\phi)) \to \infty$ and $R_c = R_d(\phi, t_0(\phi)) \to \infty$] while the liquid thickness vanishes [i.e., $R_d(\phi, t_0(\phi)) - R_b(\phi, t_0(\phi)) \to 0$]. The divergence occurs first at the triple line at $\varphi = 0$ for large CA $\theta > \pi/2$:

$$t_0(\varphi = 0) = \left(\frac{\rho_L}{6\Delta P_{\rm gr}}\right)^{1/2} R_0 \sin\theta\, \tau_0, \tag{2}$$

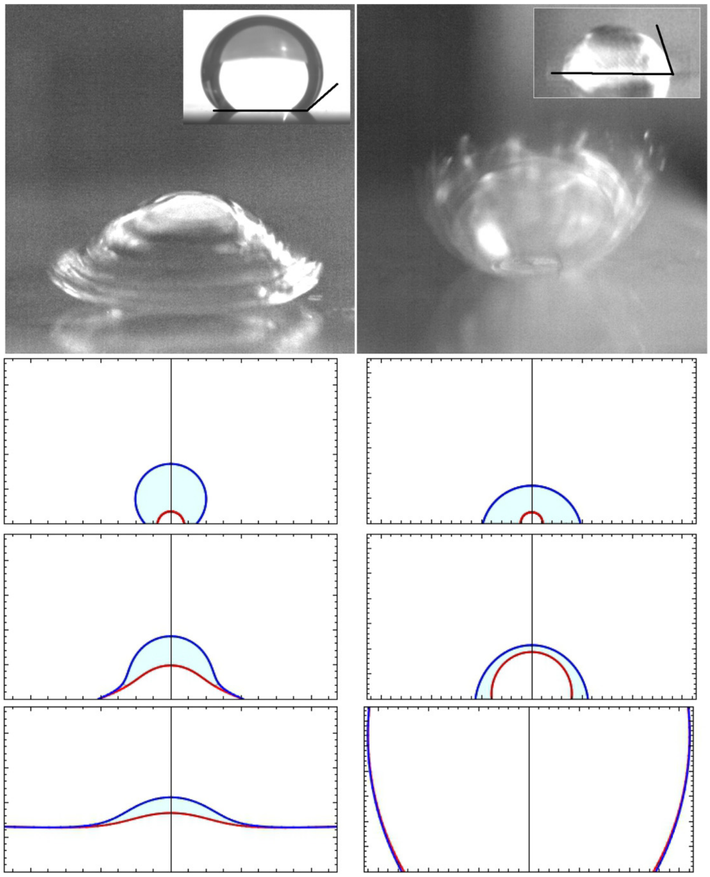

FIG. 4. Two mechanisms of vapor ejection depending on the CA in the experiments (top figures) compared to the numerical predictions (especially the bottom figures). Both insets show the drops shortly after deposition. Left: High ($\theta = 132^\circ$) CA, triple line breakup. Right: Low CA ($\theta < \pi/2$, here close to 80°), top breakup.

where $\tau_0 \approx 5.504$ is a dimensionless constant (see the Supplemental Material [18]), and R_0 is the initial drop radius. In contrast, the divergence occurs first in the vertical direction at $\varphi = \pi/2$ for small CA $\theta < \pi/2$,

$$t_0(\varphi = \pi/2) = \left(\frac{\rho_L}{6\Delta P_{\mathrm{gr}}}\right)^{1/2} R_0(1 - \cos\theta)\tau_0. \tag{3}$$

Hence, the model predicts triple-line breakup dynamics for $\theta > \pi/2$ and top-breakup dynamics for $\theta < \pi/2$.

Experiments and model are in good agreement for high CA, as shown in the left panels of Fig. 4. To check the full dynamics predicted by the model, an experiment is performed on a poorly coated sample area that exhibits a CA close to 80°. The right panels of Fig. 4 show again a satisfactory matching between experimental observation and model prediction.

Further, a quantitative comparison between the model and the experiments is shown in Fig. 5 for $\theta = 132^\circ$. The temporal evolution of the bubble height $h_b = R_b(\pi/2, t)$, of the drop height $h_d = R_d(\pi/2, t)$, and of the radius of the contact zone between the drop and the substrate $R_c = R_d(0, t)$ are confronted with the model predictions. Good agreement is obtained when choosing the bubble overpressure ΔP_{gr} as a single fit parameter. The corresponding plot of ΔP_{gr} as a function of the substrate temperature is shown in the inset of Fig. 5.

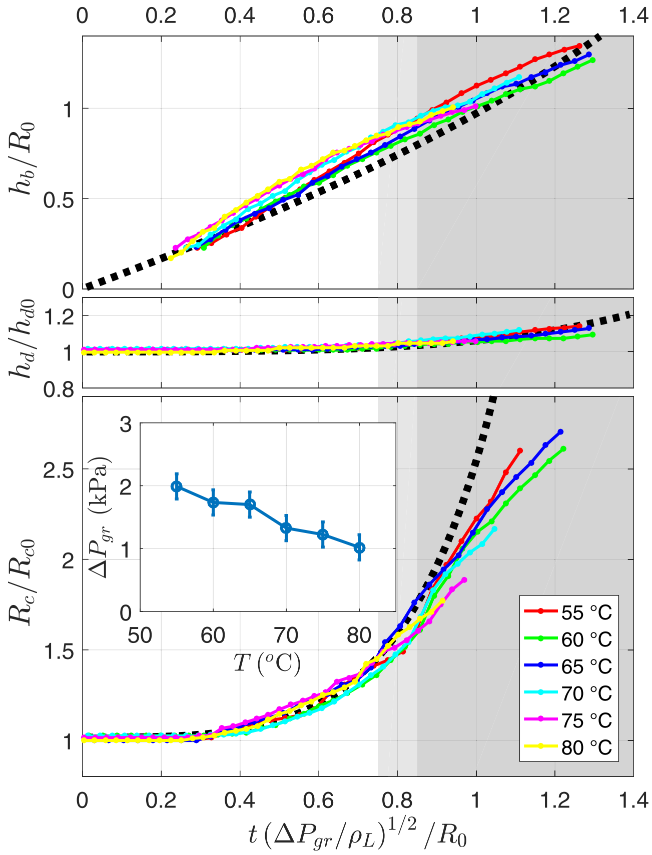

FIG. 5. Normalized bubble height h_b/R_0, drop height h_d/h_{d0}, and radius of the drop base R_c/R_{c0}, as a function of the dimensionless time. For each set, the six curves correspond to six experimental temperatures (see labels). For the three sets, the experimental curves collapse simultaneously on the black dashed master curves given by the present theory, after adjusting $\Delta P_{\mathrm{gr}}(T)$, the difference between the bubble pressure and the background pressure. Note that experiment and theory depart progressively after the time ~0.8 highlighted by the vertical light gray strip. Inset: ΔP_{gr} as a function of temperature. $\theta = 132^\circ$.

Remark that the breakup of the drop in the experiments actually occurs before the divergence predicted by the model, as the rupture of the thin liquid film at the triple line (i.e., at $\varphi = 0$) for $\theta > \pi/2$ is controlled by mechanisms that are not included in our minimal model. In the experiments, we estimate the takeoff, i.e., the detachment of the contact line, to be at the dimensionless time 0.80 ± 0.02, while the model predicts a divergence at $t_c(\phi = 0)(\Delta P_{\mathrm{gr}}/\rho_L)^{1/2}/R_0 \approx 1.7$. The experimental uncertainty results from the limited optical resolution. The difference of pressure between the bubble and the chamber vanishes $\Delta P \approx 0$ after this time, and the model is not expected to describe quantitatively the experiment beyond that point since it keeps the value ΔP_{gr}.

Although precise thermal measurements are beyond the scope of this Letter, and were not carried out, the effect of the substrate temperature on the overall dynamics is briefly discussed. It is assumed that the overpressure ΔP in the bubble, responsible for the breakup dynamics, at early stage and at first approximation is given by $\Delta P = P_{\mathrm{sat}} - P_{\mathrm{th}} - P_l$, where again P_{th} is the pressure threshold that has to be reached in the chamber to initiate the bubble expansion. P_l is the Laplace pressure in the bubble when it starts to grow. P_{sat}, the equilibrium vapor pressure in the bubble, depends on the

TABLE I. Experimental threshold pressure P_{th} inside the chamber reached when the bubble expansion starts, for the different surface temperatures, and averaged over more than ten experiments. The initial (atmospheric) pressure is 101 kPa.

T (°C)	55	60	65	70	75	80
P_{th} (kPa)	6.1 $\pm$1.2	7.8 $\pm$0.9	11.9 $\pm$1.5	17.6 $\pm$2.5	26.0 $\pm$1.2	29.4 $\pm$1.8

liquid temperature near the surface, which is supposed to be close to, but slightly below, the surface temperature.

Following the same trend as the saturation pressure P_{sat}, the experimental threshold pressure P_{th} increases with the surface temperature (see Table I). The Laplace pressure is assumed to be $P_l = 7$ kPa, as calculated from the distance between substrate pillars. The range 1–2 kPa of the overpressure, inferred from the theory as shown in the inset of Fig. 5, is recovered with P_{sat} values determined with the Clausius-Clapeyron relation (approximated with Buck equation [24]) if we assume liquid temperatures a few degrees below the surface setpoint temperatures. This lower temperature in the bubble could be interpreted as a consequence of the evaporative cooling at the drop surface before bubble growth or in the bubble during its growth. A quantitative discussion of this latter effect is reported in the Supplemental Material [18]. With the help of a simple model, we indeed recover a temperature drop of a few degrees within a small layer of the liquid in the vicinity of the bubble surface. Further detailed modeling would be required to achieve quantitative agreement and to predict the value ΔP_{gr}.

In this study, we have considered the breakup of sessile water drops through bubble expansion from air pockets initially present in the roughness of a textured surface, i.e., beneath the drop. The dynamics is triggered by the background pressure decrease. Our purely inertial model captures satisfactorily the main features in the first stage of the bubble-drop dynamics in the so-called takeoff configuration. Interestingly, it stresses a link between overpressure, i.e., burst intensity, and material temperature, in a counterintuitive way at first sight: When the breakup is triggered by the background pressure decrease, the lower the surface temperature the faster the breakup. Overall, this study could have implications in the design of heat transfer devices. Selected surface pattern, pressure, and temperature could be chosen to trigger the drop behavior and hence the heat exchange.

This research was supported by the Science and Technology Amicable Research Program (STAR) between Korea and France as Project No. 32164XB co-funded by the French Ministry of Europe and Foreign Affairs, the French Ministry for Higher Education and Research, and the National Research Foundation of Korea; and through the National Research Foundation of Korea (2020K1A3A1A21042122 and 2020R1A2C1010767).

[1] F. Celestini, T. Frisch, and Y. Pomeau, Take Off of Small Leidenfrostdroplets, Phys. Rev. Lett. **109**, 034501 (2012).

[2] P. Lecointre, T. Mouterde, A. Checco, C. T. Black, A. Rahman, C. Clanet, and D. Quéré, Ballistics of self-jumping microdroplets, Phys. Rev. Fluids **4**, 013601 (2019).

[3] J. B. Boreyko and C.-H. Chen, Self-Propelled Dropwise Condensate on Superhydrophobic Surfaces, Phys. Rev. Lett. **103**, 184501 (2009).

[4] G. Zhao, G. Zou, W. Wang, R. Geng, X. Yan, Z. He, L. Liu, X. Zhou, J. Lv, and J. Wang, Rationally designed surface microstructural features for enhanced droplet jumping and anti-frosting performance, Soft Matter **16**, 4462 (2020).

[5] C. Clanet, C. Béguin, D. Richard, and D. Quéré, Maximal deformation of an impacting drop, J. Fluid Mech. **517**, 199 (2004).
[6] C. Raufaste, G. R. Chagas, T. Darmanin, C. Claudet, F. Guittard, and F. Celestini, Superpropulsion of Droplets and Soft Elastic Solids, Phys. Rev. Lett. **119**, 108001 (2017).
[7] T. M. Schutzius, S. Jung, T. Maitra, G. Graeber, M. Köhme, and D. Poulikakos, Spontaneous droplet trampolining on rigid superhydrophobic surfaces, Nature (London) **527**, 82 (2015).
[8] M. S. Plesset and A. Prosperetti, Flow of vapour in a liquid enclosure, J. Fluid Mech. **78**, 433 (1976).
[9] C. E. Brennen, *Cavitation and Bubble Dynamics* (Cambridge University Press, Cambridge, UK, 2009).
[10] D. Obreschkow, P. Kobel, N. Dorsaz, A. de Bosset, C. Nicollier, and M. Farhat, Cavitation Bubble Dynamics Inside Liquid Drops in Microgravity, Phys. Rev. Lett. **97**, 094502 (2006).
[11] T. P. Allred, J. A. Weibel, and S. V. Garimella, Enabling Highly Effective Boiling from Superhydrophobic Surfaces, Phys. Rev. Lett. **120**, 174501 (2018).
[12] M. A. Bruning, M. Costalonga, J. H. Snoeijer, and A. Marin, Turning Drops into Bubbles: Cavitation by Vapor Diffusion Through Elastic Networks, Phys. Rev. Lett. **123**, 214501 (2019).
[13] S. T. Thoroddsen, T. G. Etoh, K. Takehara, N. Ootsuka, and Y. Hatsuki, The air bubble entrapped under a drop impacting on a solid surface, J. Fluid Mech. **545**, 203 (2005).
[14] J. T. Pham, M. Paven, S. Wooh, T. Kajiya, H.-J. Butt, and D. Vollmer, Spontaneous jumping, bouncing and trampolining of hydrogel drops on a heated plate, Nat. Commun. **8**, 905 (2017).
[15] M. Liu, H. Du, Y. Cheng, H. Zheng, Y. Jin, S. To, S. Wang, and Z. Wang, Explosive pancake bouncing on hot superhydrophilic surfaces, ACS Appl. Mater. Interfaces **13**, 24321 (2021).
[16] X. Yu, R. Hu, X. Zhang, B. Xie, and X. Luo, Explosive bouncing on heated silicon surfaces under low ambient pressure, Soft Matter **15**, 4320 (2019).
[17] R. Hatakenaka, J. Breitenbach, I. V. Roisman, C. Tropea, and Y. Tagawa, Magic carpet breakup of a drop impacting onto a heated surface in adepressurized environment, Int. J. Heat Mass Transf. **145**, 118729 (2019).
[18] See Supplemental Material http://link.aps.org/supplemental/10.1103/PhysRevFluids.8.L091601 for surface fabrication, pressure measurement, bubble visualization, details concerning the model, and a discussion on the evaporation-induced cooling down during bubble growth.
[19] P. Bourrianne, C. Lv, and D. Quéré, The cold leidenfrost regime, Sci. Adv. **5**, eaaw0304 (2019).
[20] D. Quéré, Fakir droplets, Nat. Mater. **1**, 14 (2002).
[21] S. Jung, M. K. Tiwari, N. V. Doan, and D. Poulikakos, Mechanism of supercooled droplet freezing on surfaces, Nat. Commun. **3**, 615 (2012).
[22] Y. Renardy, S. Popinet, L. Duchemin, M. Renardy, S. Zaleski, C. Josserand, M. A. Drumright-Clarke, D. Richard, C. Clanet, and D. Quéré, Pyramidal and toroidal water drops after impact on a solid surface, J. Fluid Mech. **484**, 69 (2003).
[23] L. Rayleigh, VIII. On the pressure developed in a liquid during the collapse of a spherical cavity, Lond. Edinb. Dubl. Philos. Mag. J. Sci. **34**, 94 (1917).
[24] A. L. Buck, New equations for computing vapor pressure and enhancement factor, J. Appl. Meteorol. **20**, 1527 (1981).